Cyclotron mode frequencies and resonant absorption in multi-species ion plasmas[a)]

M. Affolter,[b)] F. Anderegg, D. H. E. Dubin, and C. F. Driscoll
Department of Physics, University of California at San Diego, La Jolla, California 92093, USA

(Received 13 November 2014; accepted 15 December 2014; published online 8 April 2015)

Cyclotron mode frequencies are studied on trapped rigid-rotor multi-species ion plasmas. Collective effects and radial electric fields shift the mode frequencies away from the "bare" cyclotron frequencies $2\pi F_c^{(s)} \equiv (q_s B/M_s c)$ for each species s. These frequency shifts are measured on the distinct cyclotron modes ($m = 0, 1$, and 2) with $\cos(m\theta)$ azimuthal dependence. We find that for radially uniform plasmas the frequency shifts corroborate a simple theory expression, in which collective effects enter only through the $E \times B$ rotation frequency f_E and the species fraction δ_s. The $m = 1$ center-of-mass mode is in agreement with a simple "clump" model. Additionally, ultracold ion plasmas exhibit centrifugal separation by mass, and additional frequency shifts are observed, in agreement with a more general theory. © *2015 AIP Publishing LLC*.
[http://dx.doi.org/10.1063/1.4917177]

I. INTRODUCTION

Plasmas exhibit a variety of cyclotron modes, which are used in a broad range of devices to manipulate and diagnose charged particles. In fusion devices, cyclotron modes are used for plasma heating,[1–3] and the intensity of the plasma cyclotron emission provides a diagnostic of the plasma temperature.[4,5] Cyclotron modes in ion clouds are also widely used in molecular chemistry and biology to precisely measure ion mass. In these plasmas with a single sign of charge,[6–8] collective effects and electric fields shift the cyclotron mode frequencies away from the "bare" cyclotron frequencies $2\pi F_c^{(s)} \equiv (q_s B/M_s c)$ for each species s. Mass spectroscopy devices typically attempt to mitigate these effects with the use of calibration equations, but these equation commonly neglect collective effects[9] or conflate them with amplitude effects.[7]

Here, we quantify the shifts of cyclotron mode frequencies for several cyclotron modes varying as $\cos(m\theta - 2\pi f_m^{(s)} t)$. We also quantify the plasma heating from resonant wave absorption of the $m = 1$ center-of-mass mode. These measurements are conducted on well-controlled, laser-diagnosed, multi-species ion plasmas, with near uniform charge density n_0 characterized by the near-uniform $E \times B$ rotation frequency $f_E \equiv \mathrm{ce}n_0/B$. On these radially uniform plasmas, the cyclotron mode frequency shifts are proportional to f_E, with a constant of proportionality dependent on the species fraction $\delta_s \equiv n_s/n_0$, as predicted by a simple theory expression.[10–13] The plasma heating from resonant wave absorption is quantified using a single particle model. We find that the plasma heating and the cyclotron mode frequency shifts can be used as diagnostic tools to measure the species fractions δ_s.

The cyclotron mode frequencies are also investigated on plasmas with non-uniform species distributions $n_s(r)$. The radial distribution of species is controlled through the effects of centrifugal mass separation.[14–17] When the species are radially separated, the cyclotron mode frequencies depend on the "local" concentration of species. These measurements are in agreement with a more general theory[11,12] involving a radial integral over $n_s(r)$, with a simple asymptote for complete annular separation.

II. EXPERIMENTAL APPARATUS

These un-neutralized ion plasmas are confined in a Penning-Malmberg trap with a magnetic field of $B = 2.965 \pm 0.002$ T. A Magnesium electrode arc[18] creates a neutralized plasma, and the free electrons stream out through the +180 V end confinement potentials, leaving $N_{tot} \sim 2 \times 10^8$ ions in a cylindrical column with a length $L_p \sim 10$ cm. By use of a weak applied "rotating wall" (RW) field,[19] the ions are confined for days in a near thermal equilibrium state described by rigid rotation and a "top-hat" density profile.

Laser Induced Fluorescence (LIF) techniques[20] enable measurements of the parallel $F(\mathrm{v}_\parallel)$ and perpendicular $F(\mathrm{v}_\perp)$ velocity distributions of the Mg ions. Our "standard" plasmas with $T \sim 10^{-2}$ eV have near-uniform densities, temperatures, and $E \times B$ rotation for all species. However, the probe laser beam has a non-zero half-width of $\sigma_L = 0.39$ mm, so the LIF-measured plasma edge appears rounded. Figure 1 shows the LIF data (symbols) for $n(r)$ and $f_E(r)$, together with the expected profile (dashed) from a convolution of the laser beam with a best-fit radially uniform n_0 and f_E (solid lines). This fitting process enables accurate measurements of the rigid-rotor rotation frequency f_E and "top-hat" radius R_p which will be used to characterize the cyclotron mode frequency shifts.

The three profiles shown in Fig. 1 are of the same ions under different RW conditions. By altering the frequency of the RW field, the plasma can be re-arranged to a desired density, radius, and rotation frequency, with $n_0 R_p^2$ remaining constant. In these experiments, the ion densities range over $n_0 = (1.8 \rightarrow 6.2) \times 10^7\ \mathrm{cm}^{-3}$, with rotation

[a)]Paper DI2 4, Bull. Am. Phys. Soc. **59**, 99 (2014).
[b)]Invited speaker.

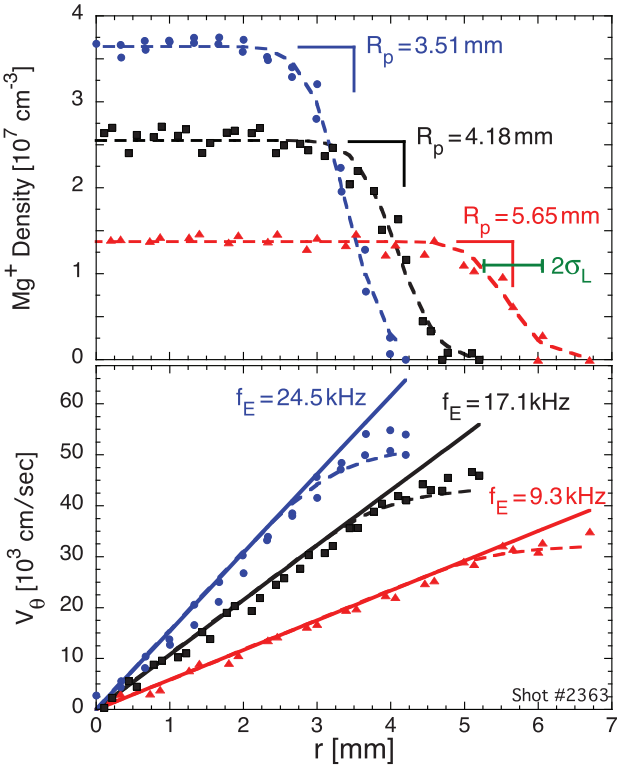

FIG. 1. Radial profiles of Mg^+ density (Top) and rotation velocities (Bottom) at three different rotation rates in the "uniform density" temperature regime $T \sim 10^{-2}$ eV. Symbols are LIF measured data convolved with the finite size probe laser beam σ_L, and dashed curves are fits to the "top-hat" rigid-rotor model (solid lines).

rates $f_E = (9 \rightarrow 30)$ kHz, and inversely varying radii $R_p = (6 \rightarrow 3)$ mm.

The plasma temperature can be controlled from $(10^{-5} \rightarrow 1)$ eV through laser cooling of the $^{24}Mg^+$. This corresponds to a several decade change in collisionality $\nu_{\perp\|} = (10^4 \rightarrow 1)\, s^{-1}$ and a Debye length $\lambda_D = (5.3 \times 10^{-3} \rightarrow 1.7)$ mm. The radial distribution of ion species is also temperature dependent through the effect of centrifugal mass separation.[14–17] For plasmas at $T \gtrsim 10^{-2}$ eV the ions species are uniformly mixed. In contrast, at $T < 10^{-3}$ eV the species begin to centrifugally separate by mass, with near-complete separation at $T < 10^{-4}$ eV.

Thermal Cyclotron Spectroscopy (TCS) is used to detect the cyclotron resonances. A cartoon of this process is shown in the inset of Fig. 2. A series of RF bursts, scanned over frequency, are applied to an azimuthally sectored confinement ring with radius $R_w = 2.86$ cm. Resonant wave absorption heats the plasma, changing the $^{24}Mg^+$ velocity distribution, which is detected through LIF diagnostics.

Figure 2 shows a broad TCS scan used to identify the plasma composition. Here, the plasma heating is detected as an increase in the cooling fluorescence, and we use a long RF burst of 10^4 cycles for a narrow frequency resolution. As expected, the plasma consists of $^{24}Mg^+$, and the Magnesium isotopes $^{25}Mg^+$ and $^{26}Mg^+$. Ions of mass 19 amu and 32 amu are also typically observed, which we believe to be H_3O^+ and O_2^+, resulting from ionization and chemical reactions with the background gas at a pressure of

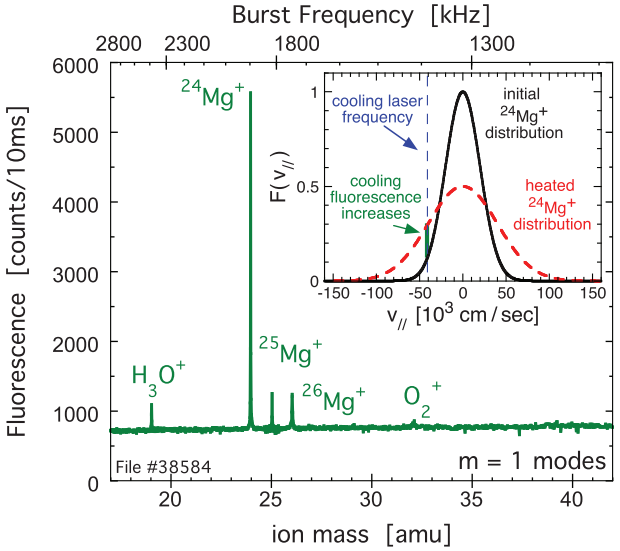

FIG. 2. Broad TCS scan of a typical plasma containing $^{24}Mg^+$, $^{25}Mg^+$, and $^{26}Mg^+$; with H_3O^+ and O_2^+ impurity ions. This mass spectra are obtained by monitoring the plasma heating from resonant wave absorption through the cooling laser fluorescence, as depicted in the inset cartoon.

$P \leq 10^{-9}$ Torr. Typical plasma isotopic charge fractions are $\delta_{24} = 0.54$, $\delta_{25} = 0.09$, $\delta_{26} = 0.10$, with the remaining 27% a mixture of H_3O^+ and O_2^+.

III. RESONANT HEATING

To quantify the resultant heating from resonant wave absorption we measure the time evolution of the parallel velocity distribution $F(v_\|, t)$ concurrent with a resonant RF burst. This entails detuning the probe laser frequency to a $v_\|$ in the Mg^+ distribution. The cooling beam is then blocked, a cyclotron mode is excited, and the arrival time of each detected photon is recorded. By repeating this process for 100 different probe detuning frequencies (i.e., parallel velocities) $F(v_\|, t)$ is measured for specified time bins. These distributions are fit by Maxwellian distributions to construct the time evolution of the plasma temperature.

Figure 3 shows the resulting temperature evolution for the excitation of the center-of-mass mode of $^{24}Mg^+$ at three different burst amplitudes A_B. In this case, the plasma is initially cooled to $T \sim 10^{-3}$ eV, and the heating due to collisions with the room temperature background gas is negligible at about 1.7×10^{-6} eV/ms. At 20 ms, the cyclotron mode is excited using a 200 cycle burst at $f_1^{(24)} = 1894.6$ kHz, corresponding to a burst period $\tau_B = 0.1$ ms. The plasma temperature increases by ΔT_s on a 10 ms time scale as the cyclotron energy is deposited as heat in the plasma, through collisions.

We find $\Delta T_s \propto (\delta_s/M_s)(A_B \tau_B)^2$ for short bursts $\tau_B \lesssim 0.1$ ms, as shown in Fig. 4. Here, the center-of-mass mode of $^{24}Mg^+$ and $^{26}Mg^+$ are excited at $f_1^{(24)} = 1894.6$ kHz and $f_1^{(26)} = 1745.2$ kHz with short bursts of 100 and 200 cycles. The amount of heating is dependent on the concentration of the species δ_s, with the majority species $^{24}Mg^+$ heating the plasma about 4× more than the minority species $^{26}Mg^+$.

This ΔT_s scaling is consistent with a single particle model. Consider an ion initially at rest in the plasma, which is then excited at the species center-of-mass cyclotron

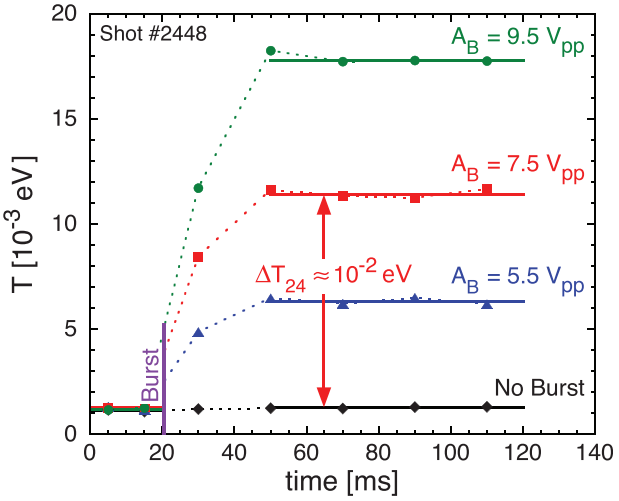

FIG. 3. Time evolution of the plasma temperature after the excitation of the center-of-mass mode of $^{24}Mg^+$ at three different burst amplitudes A_B. A 200 cycle RF burst at $f_1^{(24)} = 1894.6$ kHz is used, corresponding to a short burst period $\tau_B = 0.1$ ms.

frequency $\omega_1^{(s)} = 2\pi f_1^{(s)}$ by a sinusoidal electric field of amplitude E_0. The resulting motion can be model as an undamped driven harmonic oscillator,

$$\ddot{r} + \left[\omega_1^{(s)}\right]^2 r = \frac{q_s E_0}{M_s} \sin\left[\omega_1^{(s)} t\right]. \tag{1}$$

The amplitude of the driven cyclotron motion increases linearly in time, with an average energy in an oscillation of

$$\langle \mathcal{E}_s \rangle \propto \frac{q_s^2}{M_s} (A_B \tau_B)^2, \tag{2}$$

neglecting smaller terms linear in the burst period. Here, the strength of the electric E_0 is proportional to the burst amplitude A_B applied to an azimuthally sectored confinement ring.

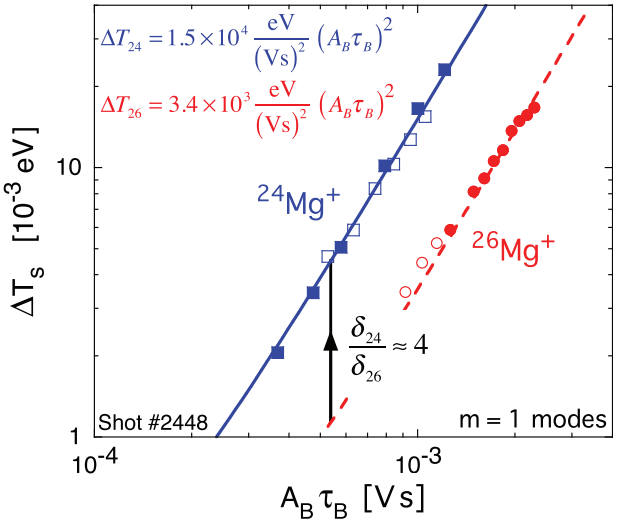

FIG. 4. Change in the plasma temperature versus burst amplitude A_B and burst period τ_B for the majority species $^{24}Mg^+$ and a minority species $^{26}Mg^+$. Open and closed symbols correspond to bursts consisting of 100 and 200 cycles, respectively.

A plasma consisting of $\delta_s N_{tot}$ identical ions, each excited by a resonant cyclotron burst to an energy $\langle \mathcal{E}_s \rangle$, will heat the plasma by $\Delta T_s \propto \delta_s (A_B \tau_B)^2 / M_s$. This model is in agreement with the measurements shown in Fig. 4. From the $(A_B \tau_B)^2$ fits, we calculate the relative concentration of the Mg^+ isotopes $\delta_{26}/\delta_{24} = (M_{26}/M_{24})(\Delta T_{26}/\Delta T_{24})$, which is within 10% of those obtained from LIF diagnostics. Thus, plasma heating from short resonant bursts enable measurements of the relative species fractions.

This model has ignored any dephasing between the oscillator and the drive, which can result from collisions, damping, or an initially off-resonant burst. Dephasing will result in less energy per ion, and as a result a smaller ΔT_s. We find that the $\Delta T_s \propto (A_B \tau_B)^2$ scaling is only valid for short bursts $\tau_B \lesssim 0.1$ ms. As the burst period is increased, keeping $A_B \tau_B$ constant, we observe a decrease in the plasma heating. At a $\tau_B \sim 1.7$ ms (~ 3000 cycles), the heating is decreased to less than 40% of the short burst expectation, with a larger decrease for the minority species.

This dephasing for long bursts explains why the height of the peaks in Fig. 2 underestimates the concentrations of the minority species. At the moment, it is unclear what is causing the dephasing on this time scale. We have changed the initial plasma temperature by an order of magnitude $(10^{-3} \rightarrow 10^{-2})$ eV to no effect, and the burst frequency is accurate to a few hundred Hz, ruling out an off-resonant drive.

IV. RADIALLY UNIFORM PLASMA

Frequency shifts are measured for the $m = 0$, 1, and 2 cyclotron modes, having density perturbations on the plasma radial surface varying as $\delta n \propto \cos(m\theta - 2\pi f_m^{(s)} t)$, as shown in Fig. 5. For the $m = 1$ center-of-mass mode, the ion orbits are in phase resulting in a displacement of the center-of-mass of the exited species, which then orbits the center of the trap at $f_1^{(s)}$, Fig. 5(a). This mode is excited by a dipole burst on an azimuthally sectored confinement ring. A quadrupole burst excites the "elliptical" $m = 2$ mode.[10,21] As shown in Fig. 5(b), this elliptical density perturbation, rotating at $f_2^{(s)}$, is created by a 180° phase shift of the ion orbits on opposite radial edges of the plasma. The final mode we have analyzed is the novel $m = 0$ radial "breathing" mode,[22–24] in which the plasma cross-section expands and contracts radially, as shown in Fig. 5(c). To excite this mode the end of the plasma is wiggled at $f_0^{(s)}$, since the wave generates no external electric field except at the plasma end. The ion orbits are typically excited to twice the thermal cyclotron radius, which at $T \sim 10^{-2}$ eV is about 40 μm.

Figure 6 shows the $m = 0$, 1, and 2 cyclotron mode frequencies for $^{24}Mg^+$. The $m = 0$ and $m = 1$ modes are downshifted from the "bare" cyclotron frequency $F_c^{(24)} = 1899.46$ kHz, while the $m = 2$ mode is upshifted. The cyclotron mode frequencies are measured from the peaks in this heating response to an accuracy of approximately 100 Hz. The difference in frequency between these modes closely equals the measured $E \times B$ rotation frequency $f_E = 9.3$ kHz. We note that the width of these resonances is a possible measurement of the mode damping γ.

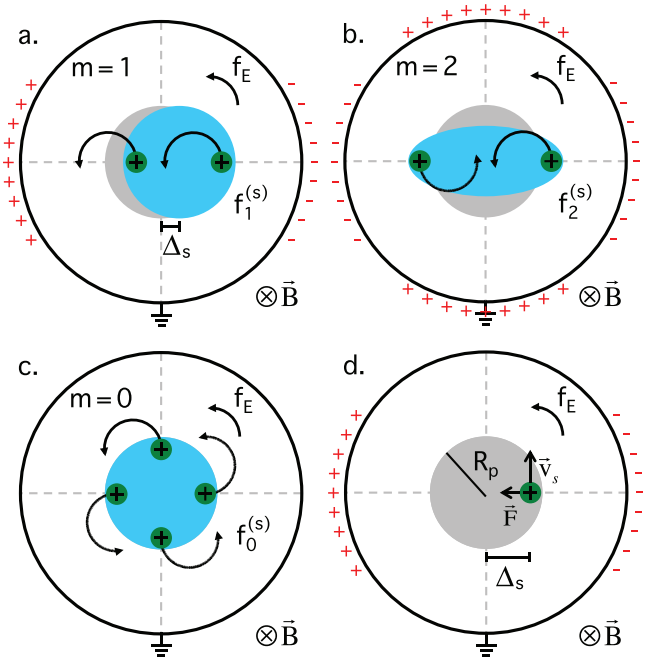

FIG. 5. Sketches of the $m = 1$, 2, and 0 surface waves (a)-(c); and simple clump model (d). The cyclotron mode frequencies are shifted proportional to the $E \times B$ drift-rotation frequency f_E, arising from the *non-resonant* species, image charges on the trap wall, and trap potentials.

In the case of the $m = 1$ mode, this downshift away from the "bare" cyclotron frequency can be understood through a simple clump model. Sketched in Fig. 5(d) is a cylindrical trap confining a multi-species ion plasma. A species is excited to an amplitude Δ_s, and undergoes uniform circular motion about the center of the trap with a velocity v_s, resulting in a frequency $f_1^{(s)} = v_s/2\pi\Delta_s$. The dynamics of this excited species can be modeled by a point particle located at the center-of-mass of the excited species. The radial forces acting on this point particle are the centrifugal, $v_s \times B$, and electrostatic forces, summing to zero as

$$\frac{M_s v_s^2}{\Delta_s} - \frac{q_s}{c} v_s B_z + q_s \tilde{E}_r = 0. \tag{3}$$

Here, $\tilde{E}_r$ represents the electric field of the *non-resonant* species, trap potentials, and image charge on the trap wall; rather than the total electric field E_r measured through f_E. Equation (3) reduces to $f_1^{(s)} = F_c^{(s)}$ when $\tilde{E}_r = 0$. However, in general, radial electric fields reduce the radial forces, causing a downshift in the center-of-mass mode frequency.

In these experiments, the radial electric field is controlled by compressing the plasma with the RW, and the strength of this electric field is measured through the $E \times B$ rotation frequency f_E. In Fig. 7, the measured cyclotron frequencies of the $m = 0$, 1, and 2 modes are plotted versus f_E for the majority species $^{24}Mg^+$ and a minority species $^{26}Mg^+$. The cyclotron mode frequency shifts are proportional to f_E, but the proportionality constants are different for the majority species $^{24}Mg^+$, than for the minority species $^{26}Mg^+$, due to plasma collective effects.

These cyclotron mode frequencies can be obtained from plasma wave theory. This theory assumes a cold, radially uniform plasma of infinite length, and solves the Vlasov-Poisson equation for a $\cos(m\theta)$ surface perturbation in a frame rotating with the plasma at f_E. Frequency shifts of the form

$$f_m^{(s)} - F_c^{(s)} = [(m-2) + \delta_s(1 - \mathcal{R}_m)]f_E, \tag{4}$$

are predicted.[11,12,25] The $\delta_s(1 - \mathcal{R}_m)f_E$ term represents collective interactions in the plasma frame rotating at f_E; the $-2f_E$ term is a shift due to the Coriolis force in the plasma frame; and the mf_E term is the Doppler shift back to the lab frame. For $m \geq 1$, the wall image charge correction is $\mathcal{R}_m \equiv (R_p/R_w)^{2m}$, but $\mathcal{R}_m \equiv 0$ for $m = 0$. The $\delta_s f_E = (f_p^{(s)})^2/2F_c^{(s)}$ shifts reflects plasma frequency f_p restoring forces, as seen in the upper-hybrid modes with $f_{uh}^2 = F_c^2 + f_p^2$.

For the $m = 1$ mode, surface wave theory predicts a frequency shift of $(\delta_s - 1)f_E - \delta_s(R_p/R_w)^2 f_E$. This frequency shift can be interpreted from the simple clump model. The $(\delta_s - 1)f_E$ term represents the radial electric field from the *non-resonant* species. A species center-of-mass cannot exert a force on itself, reducing the effective space charge electric field by δ_s. However, the image charges of the excited species *do* exert a force on its own center-of-mass, represented here by a frequency shift of $f_D^{(s)} = \delta_s(R_p/R_w)^2 f_E$, equal to the species $m = 1$ diocotron frequency. In these experiments $R_p \ll R_w$, so the dominant frequency shift is caused by the *non-resonant* species. The image charge frequency shift $f_D^{(s)} < 200$ Hz, depending on the concentration of the species.

Fitting Eq. (4) to the measured frequency shifts in Fig. 7, we find that the observed mode frequency spacing is consistent to within the 2% accuracy of the LIF measurements of f_E, and that these cyclotron modes converge to the "bare" cyclotron frequency $F_c^{(s)}$ in the limit $f_E \to 0$. Also, the slope of the frequency shifts in Fig. 7 provides a measurement of the species fractions δ_s for each species. The relative fraction of the Mg^+ isotopes δ_{26}/δ_{24} is within 20% of those obtained through LIF diagnostics and within 5% of that

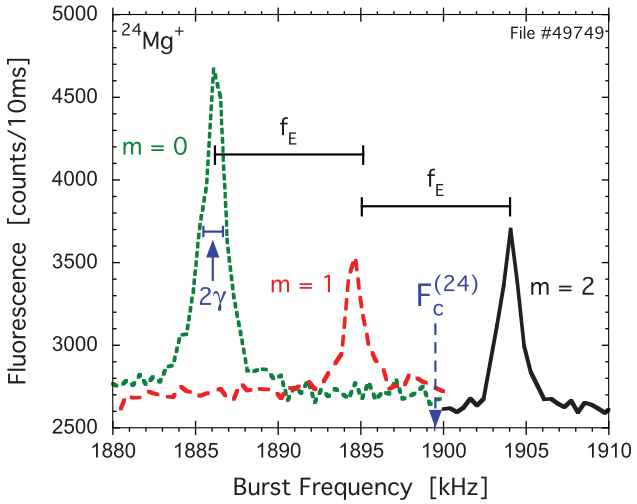

FIG. 6. Observed $^{24}Mg^+$ cyclotron resonances for $m = 0$, 1, and 2 modes. Modes are shifted away from the "bare" cyclotron frequency $F_c^{(24)} = 1899.46$ kHz. These modes have a frequency spacing of approximately the $E \times B$ rotation frequency $f_E = 9.3$ kHz.

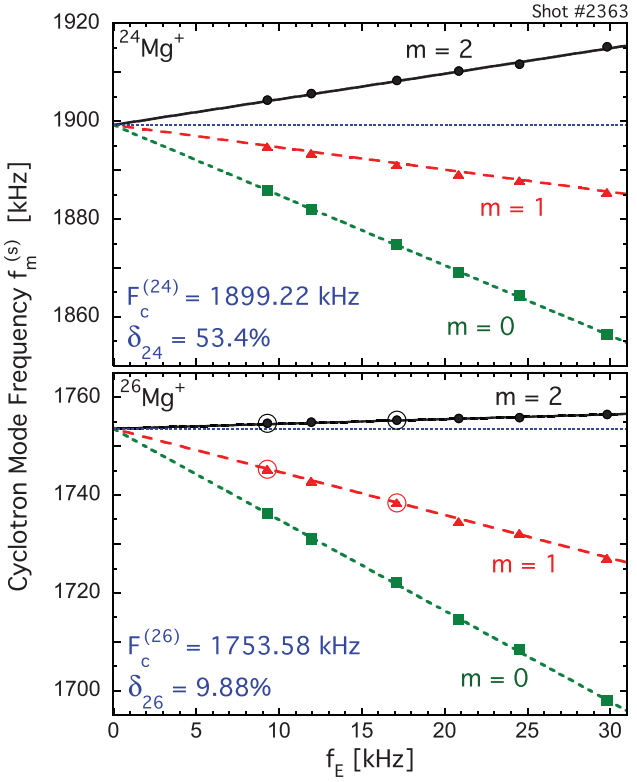

FIG. 7. Cyclotron mode frequencies versus measured f_E for the majority species $^{24}Mg^+$, and a minority species $^{26}Mg^+$. Symbols are experimental data and curves are fits to Eq. (4), which determine $F_c^{(s)}$ (dotted) and δ_s for each species.

obtained from the resonant wave absorption technique. The corresponding mass ratio from $F_c^{(s)}$ is accurate to within 200 ppm. A similar agreement is found for δ_{25}/δ_{24}.[13]

Four frequencies $f_m^{(s)}$ from two m-theta modes in two plasma states could be used to determine the plasma characteristics f_E and δ_s, and thereby determine $F_c^{(s)}$. In Fig. 7, the measured cyclotron frequency differences of the two circled (vertical) data pairs give $f_E = (9.33, 16.97)$ kHz versus the measured $(9.29, 17.13)$ kHz; and Eq. (4) then gives $\delta_{26} = 9.06\%$ and $F_c^{(26)} = 1753.82$ kHz, in close agreement with the results in Fig. 7. Of course, similar information from multiple species would improve this plasma characterization.

This surface wave theory[11,12,25] has ignored finite length effects resulting from the trap end potentials. These effects have been measured on the low-frequency diocotron mode in electron plasmas.[26] Extending these results to the plasma conditions of our experiments, we find that finite length effects produce a frequency shift of approximately 50 Hz, which is small compared to the frequency shift of the *non-resonant* species.

In a single species plasma ($\delta = 1$), the frequency shifts from trap potential and image charge are dominant, since there are no *non-resonant* species. Prior work[21] measured the center-of-mass cyclotron mode frequency on electron plasmas and found that the $m = 1$ mode is downshifted by the diocotron frequency f_D, due to image charge in the conducting walls. Later multi-species work[10] described the spacing between the m-modes in terms of several f_D when image charges dominated. This prior work was conducted on hot plasmas $T \sim 3$ eV, with parabolic density profiles, and large R_p/R_w. In general, f_E is the more fundamental parameter describing these frequency shift, having little to do with R_w.

V. NON-UNIFORM SPECIES FRACTIONS

In this section, we investigate the cyclotron mode frequencies on plasmas with non-uniform species fractions. The radial distribution of species is controlled through the effects of centrifugal mass separation. When uniformly distributed, species of different mass rotate at slightly different rates and therefore experience a viscous drag in the azimuthal direction. This drag produces an $F_{drag} \times B$ drift, which radially separates the species to form a rigid-rotor rotation profile. The species concentrate into separate radial annuli, each approaching the full plasma density n_0, with the lighter species on center.

The equilibrium density profiles of each species can be theoretically determined. The ratio of densities between two species is equal to

$$\frac{n_a(r)}{n_b(r)} = C_{ab} \exp\left[\frac{1}{2T}(m_a - m_b)(2\pi f_E)^2 r^2\right], \qquad (5)$$

where C_{ab} is a constant determined by the overall fraction of each species.[17] The effects of centrifugal mass separation are important for species with a large mass difference and for cold plasmas.

Shown in Fig. 8 are measured density profiles for both a warm plasma with minimal separation and a cold plasma with strong separation. The symbols represent the LIF measured

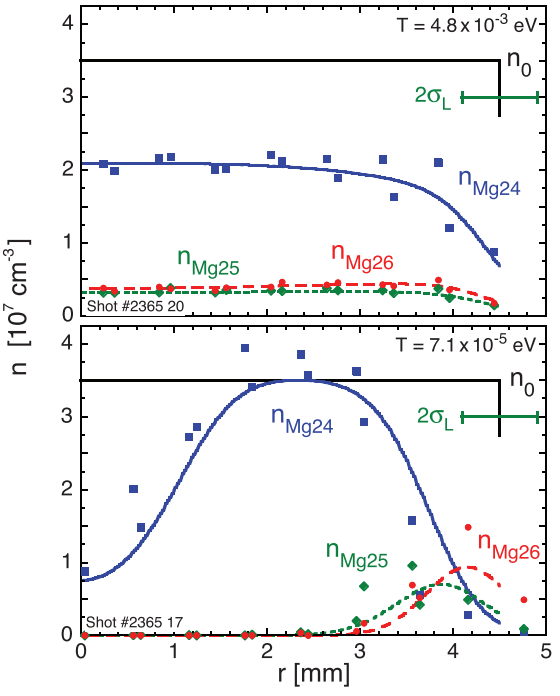

FIG. 8. Radial density profiles of both a warm (top) and a cold (bottom) plasma. Symbols are the measured laser-width averaged data, and solid black lines represent the total plasma density n_0 measured through f_E. The curves are theory predicted profiles resulting from Eq. (5), with measured $f_E = 17.0$ kHz, $R_p = 4.5$ mm, $M_s = (24, 25, 26, 19, 32)$ amu, and $\delta_s = (54, 9, 12, 8, 17)\%$.

densities of the Mg^+ isotopes, and the solid black line is the total plasma density n_0 measured through the $E \times B$ rotation frequency. The curves are theory predicted profiles for the measured species fractions δ_s, plasma rotation frequency f_E, and "top-hat" radius R_p. These theory profiles have been convolved with the finite size probe laser beam σ_L, so they can be compared directly with the experimental measurements.

At $T = 4.8 \times 10^{-3}$ eV, the species are uniformly mixed, as shown in Fig. 8 (top). This is a typical example of a radially uniform plasma. Here, the species fractions $\delta_s \equiv n_s/n_0$ are constant over the plasma radius, and the cyclotron mode frequencies are well described by Eq. (4). Note that the sum of the Mg^+ isotopes is not equal to the total plasma density due to the presence of impurity ions, H_3O^+ and O_2^+, not detected by the LIF diagnostics.

As the plasma is cooled, the species centrifugally separate and concentrate into radial annuli, increasing the "local" $n_s(r)$. At $T = 7.1 \times 10^{-4}$ eV, the $^{24}Mg^+$ has approached the full plasma density n_0, pushing the heavier Mg^+ isotopes to the radial edge, as shown in Fig. 8 (bottom). The central hole observed in the Mg^+ density profile is a result of the lighter impurity species H_3O^+. Although the overall species fractions are unchanged, the "local" $\delta_s(r) \equiv n_s(r)/n_0$ have increased for each species. We find that the cyclotron mode frequencies are dependent on these "local" species fractions.

Shown in Fig. 9 are measurements of the $m = 1$ frequency shifts as the "local" species concentrations are varied by altering the plasma temperature. These shifts are measured on $^{24}Mg^+$, $^{26}Mg^+$, and H_3O^+. At $T \gtrsim 10^{-3}$ eV, the species are uniformly mixed and the frequency shifts are approximately $(\delta_s - 1)f_E$, as predicted by Eq. (4).

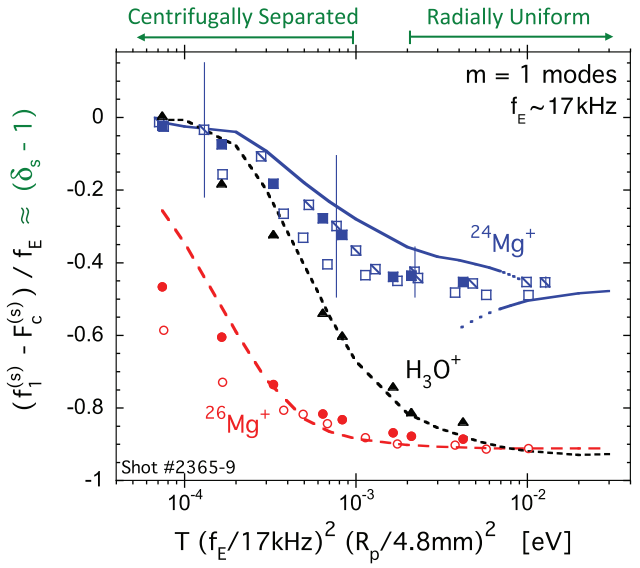

FIG. 9. Normalized shifts of the $m = 1$ cyclotron mode frequencies for $^{24}Mg^+$, $^{26}Mg^+$, and H_3O^+, as the "local" species concentrations increase due to centrifugal separation. Symbol shapes represent species; symbol fill distinguishes measurements on three plasmas with slightly different compositions. The temperature T is scaled by the centrifugal energy of these plasmas, which differ by approximately 25%. Curves are theory predictions assuming a typical species concentration $M_s = (24, 25, 26, 19, 32)$ amu with $\delta_s = (54, 9, 9, 8, 20)\%$. The four vertical lines are the FWHM of the $^{24}Mg^+$ cyclotron resonance at various temperatures.

Cooling the plasma increases the "local" species concentrations and decreases the $m = 1$ frequency shift. At the coldest temperatures $T \sim 10^{-4}$ eV, the $^{24}Mg^+$ and H_3O^+ have approached the full plasma density n_0, and the center-of-mass cyclotron mode frequency is nearly the "bare" cyclotron frequency. Similar frequency shifts are observed for both the $m = 0$ and $m = 2$ modes, offset by $(m-1)f_E$.

For radially varying ion densities $n_s(r)$ or varying rotation $f_E(r)$, the mode resonances at $f_m^{(s)}$ are predicted by peaks in the real part of the admittance $Re(Y_m)$.[11] Here, $Y_m \equiv I/V$ relates electrode displacement current to electrode voltage. It has a frequency dependence of

$$Y_m \propto i(2\pi f)\frac{G_m + 1}{G_m - 1}, \tag{6}$$

with

$$G_m \equiv -\frac{2m}{R_w^{2m}}\int_0^{R_w} dr\, \frac{\beta(r)\, r^{2m-1}}{\alpha(r) - \beta(r)}, \tag{7}$$

$$\beta(r) \equiv \frac{n_s(r)}{n_0} f_E(0), \tag{8}$$

and

$$\alpha(r) \equiv \left(f_m^{(s)} - F_c^{(s)} + i\gamma/2\pi\right) - (m-2)f_E(r) + \frac{r}{2}\frac{\partial}{\partial r} f_E(r). \tag{9}$$

Peaks in $Re(Y_m)$ occur when $G_m \to 1$.

The curves in Fig. 9 are the shifts resulting from numerically integrating Eq. (6) with $n_s(r)$ as predicted for centrifugal separation, Eq. (5). As the plasma is cooled, the "local" $n_s(r)$ increases towards the full "top-hat" density n_0 isolating the species and thus removing the frequency shift from the *non-resonant* species. The cyclotron mode frequencies as a result are then shifted towards the single-species $\delta_s = 1$ limit. Here, the remaining shifts due to image charge[12] and trap electric fields are negligible. The discontinuity in the $^{24}Mg^+$ theory curve is due to multiple modes with different radial mode structure. Although multiple radial modes have been observed on some plasmas, they were not observed for this set of data, possibly due to stronger damping.

Varying the plasma temperature also changes the width of the cyclotron resonance, as shown by the four vertical *FWHM* (2γ) bars in Fig. 9. At high temperatures $T \gtrsim 10^{-2}$ eV, the resonance width is at least the frequency width of the drive, which is approximately 0.4 kHz. When the plasma is cooled, the ion-ion collision frequency increases, and the resonance width increases with the same qualitative behavior. For $T \lesssim 10^{-3}$ eV, inter-species collisions are reduced by centrifugal separation of the species, and the cyclotron resonance width is observed to remain constant at approximately 6 kHz.

At temperatures $T \gtrsim 0.1$ eV where ion-ion collisionality is small, we observed multiple closely spaced modes with spacing dependent on T. This mode splitting is similar to that observed in electron plasmas;[21] but here this splitting occurs for the $m = 1$ mode which was not previously seen. Recent theory[12] involving radially standing Bernstein waves in

multi-species ion plasmas predicts a similar frequency spacing, and a connection to this theory is being pursued.

VI. CONCLUSION

On radially uniform plasmas the cyclotron mode frequencies are shifted by radial electric fields and collective effects in agreement with surface wave theory, Eq. (4). These frequency shifts can be used to measure the plasma $E \times B$ rotation frequency f_E, and species fractions δ_s. This quantitative understanding of the frequency shifts give a physical basis for the "space charge" and "amplitude" calibration equations commonly used in mass spectroscopy.[27] For short bursts $\tau_B \lesssim 0.1$ ms, the plasma heating from resonant wave absorption of the $m = 1$ mode is found to be $\Delta T_s \propto \delta_s A_b^2 \tau_b^2 / M_s$, providing another diagnostic tool of δ_s. For non-uniform plasmas, the cyclotron mode frequencies are dependent on the "local" species concentrations, and the frequency shifts from *non-resonant* species are removed when the excited species is completely separated.

ACKNOWLEDGMENTS

This work was supported by National Science Foundation grant PHY-1414570, and Department of Energy Grant Nos. DE-SC0002451 and DE-SC0008693.

[1]J. Adam, Plasma Phys. Controlled Fusion **29**, 443 (1987).
[2]R. Gilgenbach, M. Read, K. Hackett, R. Lucey, B. Hui, V. Granatstein, K. Chu, A. England, C. Loring, O. Eldridge, H. Howe, A. Kulchar, E. Lazarus, M. Murakami, and J. Wilgen, Phys. Rev. Lett. **44**, 647 (1980).
[3]H. Laqua, V. Erckmann, H. Hartfuß, H. Laqua, and W7-AS ECRH Group, Phys. Rev. Lett. **78**, 3467 (1997).
[4]F. Volpe, H. Laqua, and W7-AS Team, Rev. Sci. Instrum. **74**, 1409 (2003).
[5]G. Taylor, P. Efthimion, B. Jones, T. Munsat, J. Spaleta, J. Hosea, R. Kaita, R. Majeski, and J. Menard, Rev. Sci. Instrum. **72**, 285 (2001).
[6]M. Easterling, T. Mize, and I. Amster, Anal. Chem. **71**, 624 (1999).
[7]C. Masselon, A. Tolmachev, G. Anderson, R. Harkewicz, and R. Smith, J. Am. Soc. Mass Spec. **13**, 99 (2002).
[8]R. Wong and I. Amster, Int. J. Mass Spec. **265**, 99 (2007).
[9]E. B. Ledford, D. L. Rempel, and M. L. Gross, Anal. Chem. **56**, 2744 (1984).
[10]E. Sarid, F. Anderegg, and C. F. Driscoll, Phys. Plasmas **2**, 2895 (1995).
[11]R. W. Gould, Phys. Plasmas **2**, 1404 (1995).
[12]D. H. Dubin, Phys. Plasmas **20**, 042120 (2013).
[13]M. Affolter, F. Anderegg, D. Dubin, and C. Driscoll, Phys. Lett. A **378**, 2406 (2014).
[14]T. O'Neil, Phys. Fluids **24**, 1447 (1981).
[15]D. Larson, J. Bergquist, J. Bollinger, W. M. Itano, and D. Wineland, Phys. Rev. Lett. **57**, 70 (1986).
[16]G. Andresen, M. Ashkezari, M. Baquero-Ruiz, W. Bertsche, P. Bowe, E. Butler, C. Cesar, S. Chapman, M. Charlton, A. Deller, S. Eriksson, J. Fajans, T. Friesen, M. Fujiwara, D. Gill, A. Gutierrez, J. Hangst, W. Hardy, M. Hayden, A. Humphries, R. Hydomako, S. Jonsell, N. Madsen, S. Menary, P. Nolan, A. Olin, A. Povilus, P. Pusa, F. Robicheaux, E. Sarid, D. Silveira, C. So, J. Storey, R. Thompson, D. van der Werf, J. Wurtele, and Y. Yamazaki, Phys. Rev. Lett. **106**, 145001 (2011).
[17]D. H. Dubin, in *NON-NEUTRAL PLASMA PHYSICS VIII: 10th International Workshop on Non-Neutral Plasmas* (AIP Publishing, 2013), Vol. 1521, pp. 26–34.
[18]R. A. MacGill, I. G. Brown, and J. E. Galvin, Rev. Sci. Instrum. **61**, 580 (1990).
[19]F. Anderegg, E. Hollmann, and C. Driscoll, Phys. Rev. Lett. **81**, 4875 (1998).
[20]F. Anderegg, X.-P. Huang, E. Sarid, and C. F. Driscoll, Rev. Sci. Instrum. **68**, 2367 (1997).
[21]R. W. Gould and M. A. LaPointe, Phys. Rev. Lett. **67**, 3685 (1991).
[22]S. Barlow, J. Luine, and G. Dunn, Int. J. Mass Spec. Ion Process. **74**, 97 (1986).
[23]D. Rempel, E. Ledford, Jr., S. Huang, and M. Gross, Anal. Chem. **59**, 2527 (1987).
[24]A. Peurrung, R. Kouzes, and S. Barlow, Int. J. Mass Spec. Ion Process. **157**, 39 (1996).
[25]R. C. Davidson, *Physics of Nonneutral Plasmas* (Addison-Wesley New York, 1990), Vol. 5, Chap. 5.6.1.
[26]K. S. Fine and C. F. Driscoll, Phys. Plasmas **5**, 601 (1998).
[27]M. Affolter, F. Anderegg, and C. Driscoll, J. Am. Soc. Mass Spec. **26**, 330 (2015).